Materials and Structures (2025) 58:204
https://doi.org/10.1617/s11527-025-02729-3

ORIGINAL ARTICLE

Low-carbon calcined clay-based binders for sustainable hempcrete

Siddharth Girish Nair · Quang Dieu Nguyen · Qiaoxi Zhu · Mahmoud Karimi · Yixiang Gan · Haiyi Zhong · Arnaud Castel · Peter J. Irga · Cecilia Gravina da Rocha · Fraser R. Torpy · Sara Wilkinson · Danielle Moreau · Fabien Delhomme

Received: 27 September 2024 / Accepted: 5 July 2025

Abstract The building sector is responsible for approximately 40% of total anthropogenic greenhouse gas emissions and 37% of global energy consumption. Hempcrete, fabricated from industrial hemp, can offer a tremendous potential to alleviate the carbon emissions and energy usage from buildings and construction based on its carbon capture and storage capability and low thermal conductivity. However, conventional lime-based binders for hempcrete are carbon intensive. This study investigates three low carbon binder alternatives for hempcrete: HL-Ref (100% hydrated lime), HL–CC (50% hydrated lime, 50% calcined clay), HL–CC–LS (50% hydrated lime, 50% calcined clay and limestone), Geo-CC [geopolymer binder with 70% calcined clay and 30% granulated ground blast furnace slag (GGBFS)]. Compressive strength, bulk density, sound absorption coefficient, thermal conductivity, surface bond strength and crystalline phases of hempcrete were assessed and a multicriteria analysis was carried out to compare the hempcrete performance between different mix designs. Results showed that the Geo-CC hempcrete using the calcined clay/GGBFS geopolymer binder achieved the best performance in terms of compressive strength, surface bonding capacity and thermal conductivity. The performance of HL–CC–LS hempcrete also achieved outstanding properties which could not be achieved by using only calcined clay (HL–CC), highlighting the beneficial synergy between limestone and calcined clay in a lime-based system. The HL–CC–LS hempcrete achieved the best acoustic performance with the highest sound absorption coefficient.

S. G. Nair · Q. D. Nguyen (✉) · A. Castel · P. J. Irga · C. G. da Rocha
School of Civil and Environmental Engineering, University of Technology Sydney (UTS), Sydney, NSW 2007, Australia
e-mail: quangdieu.nguyen@uts.edu.au

Q. Zhu · M. Karimi
School of Mechanical and Mechatronic Engineering, University of Technology Sydney (UTS), Sydney, NSW 2007, Australia

Y. Gan · H. Zhong
School of Civil Engineering, University of Sydney, Sydney, NSW, Australia

F. R. Torpy
School of Life Sciences, University of Technology Sydney (UTS), Sydney, NSW 2007, Australia

S. Wilkinson
School of Built Environment, University of Technology Sydney (UTS), Sydney, NSW 2007, Australia

D. Moreau
School of Mechanical and Manufacturing Engineering, UNSW Sydney, Sydney, NSW, Australia

F. Delhomme
University of Lyon, INSA-Lyon, GEOMAS, Villeurbanne, France

Published online: 21 July 2025

Keywords Hempcrete · Calcined clay · Limestone · Geopolymer · Sound absorption · Thermal conductivity

1 Introduction

The building sector, including both the construction phase and operational phase, is responsible for approximately 40% of total anthropogenic greenhouse gas (GHG) emissions and 37% of global energy consumption [1]. In Australia, the construction sector accounts for 18% of GHG emissions and 38% of national waste [2, 3]. Greenhouse gas emissions which result in global warming and the gradual exhaustion of natural resources contribute to the degradation of the environment [4]. Construction materials produce emissions which are a significant contributor to global carbon emissions. Specifically, the production of cement, which is the main component of concrete, accounts for 5–8% of total GHG emission [5]. The implementation of environment friendly materials plays a crucial role in reducing the embodied and overall carbon footprint of the building sector. Sustainable construction materials can offer advantages such as reducing the energy consumption, a minimal dependence on natural resources and alleviating the negative impacts on the environment [6]. Over the years, several efficient materials have been developed exhibiting various mechanical, acoustic and thermal properties [7–9]. The utilisation of bio-based construction materials, especially for the thermal insulation, is observed to be an effective method for minimising the environmental impacts of the built environment [10, 11]. Hempcrete, fabricated from industrial hemp, is considered as a potential alternative to traditional building materials for its versatility, rapid production cycle and least carbon output [12–14]. Due to the biogenic carbon sequestration of hemp during its growth cycle, hempcrete is a low embodied energy (EE) and a negative embodied carbon (EC) material [15]. Biogenic carbon sequestration refers to the process of capturing and storing atmospheric carbon dioxide (CO_2) through the growth of plants, such as hemp. While hempcrete has the potential to be a low-embodied-energy material, it is not automatically so. The energy required to produce hempcrete depends on the methods used for cultivating hemp, processing hemp hurds, and manufacturing the binder (e.g., lime or geopolymer). Efficient production methods can significantly reduce embodied energy and embodied carbon [16]. Embodied energy refers to the total energy required to produce a material, including raw material extraction, transportation, manufacturing, and construction. For hempcrete, this includes the energy used to grow, harvest, and process the hemp, as well as the production of the lime binder and the creation of the final product [17]. The connection between biogenic carbon sequestration and embodied carbon lies in the fact that hempcrete may have a negative net carbon footprint due to the carbon absorbed during hemp's growth phase. Essentially, the carbon captured by the hemp plant can offset the embodied carbon involved in producing the material, potentially making hempcrete a carbon-negative material. However, this outcome depends on several key factors, such as local sourcing, processing of hemp hurds, mixing of different additives into types of hempcretes, transportation, lime binder production and availability, supply chains, and the availability of mass-scale production units.

The acoustic and thermal performances of hemp based composite materials can be studied by analysing the sound absorption coefficient and thermal conductivity. Fernea et al. studied the sound absorption properties and thermal conductivity of hemp-based materials by dividing the experiments into monolayer and multilayer fibre [18]. The results showed that the incorporation of hemp improved both thermal and acoustic performance of the material. It was also reported that hemp-lime and hemp-clay demonstrated similar acoustic behaviour using the impedance tube test and that the hemp to binder ratio is an important parameter governing the acoustic properties of bio-based concrete [19]. Hempcrete has been a promising carbon-negative and energy efficient non-load bearing material in some regions such as European countries, but most of its full potential as a sustainable carbon sequestering construction material is not completely still explored [20–22].

Hempcrete is already a low embodied carbon construction material as a result of carbon storage during hemp growth, and the low quantity of binder required compared to traditional concrete. Two types of binder are commonly used in hempcrete: Ordinary Portland Cement (OPC) or lime. The manufacturing process of both OPC and lime is instinctively carbon-intensive because it involves

the thermal decarbonisation of limestone, releasing CO_2 into the atmosphere [23, 24]. Supplementary cementitious materials (SCMs) such as ground granulated blast furnace slag (GGBFS), clay or metakaolin blended with OPC or lime, have been successfully considered as alternative binders to further reduce hempcrete's global warming potential (GWP) while retaining its favourable mechanical, moisture and thermal quality [17, 18]. Degrave-Lemeurs et al. [19] also reported that hemp-clay composites have a significantly lower embodied carbon and energy than hemp-lime composites. Alkali-activated materials i.e., geopolymer have been also considered to manufacture hempcrete [25, 26].

In this study, to enhance the sustainability and accelerate the adoption of hempcrete technology by the construction industry, three low carbon binders were investigated. Calcined clay, which has been attracting significant worldwide attention as an emerging SCM [27], is utilised as one of the main components in the low-carbon binders. The first binder is a blend of 50 wt.% hydrated lime and 50 wt.% calcined clay. The second one is a blend of 17 wt.% limestone, 33 wt.% calcined clay and 50 wt.% hydrated lime. This binder was similar to limestone calcined clay cement (LC3) that has been successfully used in traditional OPC-based concrete [28, 29]. However, the hydrated lime was employed instead of OPC as in the LC3 system as hydrated lime manufacture produces less CO_2 emission than OPC [24]. The third low-carbon binder is a geopolymer binder activated using a sodium hydroxide and sodium silicate solution. The precursor used is a blend of 70 wt.% calcined clay and 30 wt.% GGBFS which has also been successfully used in traditional concrete applications [30–34]. Compressive strength, bulk density, surface bond strength, acoustic and thermal properties for each hempcrete composite were investigated in this study. The acoustic and thermal properties were evaluated by sound absorption coefficient and thermal conductivity respectively. XRD analysis was conducted in binder pastes to reveal the reaction products affecting the properties of the different hempcrete mixes. Finally, a multicriteria analysis was discussed to elaborate on the advantages of hempcrete with low-carbon binders.

2 Materials and mix designs

2.1 Hemp hurds characterisation

The stem component of the industrial hemp, which has undergone the process of retting also known as hemp hurds, has been used for the study. The hemp hurds are locally sourced by the Australian Hemp Masonry Company Pty. Ltd. The particle size distribution of the hemp hurds, measured using the sieve analysis recommended by RILEM TC 236-BBM [35], is presented in Fig. 1. The particle size distribution of the hemp hurds in this study is finer than that of the Australian hurds used by Delhomme et al. [13] with more particles passing within the range 0.6–4.74 mm.

The water absorption of the hemp hurds, including initial water content (INC) and final water content (FWC), was assess using a "salad spinner" following the recommendations of the RILEM TC 236-BBM [35]. The water absorption results, from 1 min to 48 h, obtained on three specimens are presented in Fig. 2. In the previous study conducted by Delhomme et al. [13], a very significant specimen mass increase was observed between 4 and 48 h, whereas the hemp hurds used in this study show a small increment of mass after 4 h

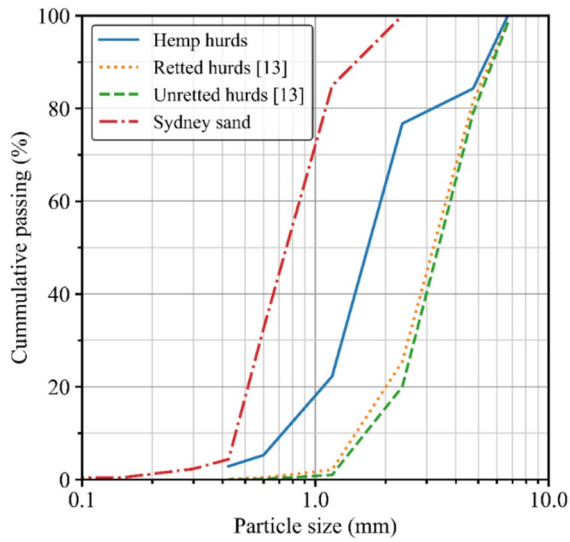

Fig. 1 Gradation, i.e., particle size distribution of hemp hurds (compared to hemp hurds in the previous study [13]), and Sydney sand

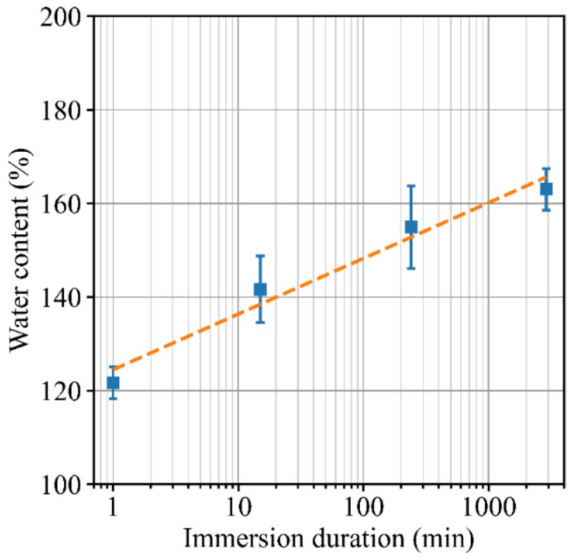

Fig. 2 Water absorption of hemp hurds

or 1 day (Fig. 2). The 1-min initial water content (INC) measured by Delhomme et al. [13] was 165–190%. The INC ranged between 118 to 130% in this study. Regarding the 48 h immersion, the final water content (FWC) values measured by Delhomme et al. [13] ranged from 354 to 387%. The FWC values obtained in this study range between 158 and 165%. As a result, the water absorption of the hemp hurds used in this study is overall significantly lower than the water absorption of the hemp hurds used in a previous study by the authors [13]. The influence of hemp hurds water absorption on hempcrete properties will be discussed in Sect. 4.

2.2 Binders

Four different binders were used in this study to investigate their effects on hempcrete performance. The binder of the reference mix is 100 wt.% hydrated lime, which was supplied by Australian Hemp Masonry Company Pty. Ltd. For two of the low-carbon binders, hydrated lime was replaced by calcined clay and limestone up to 50 wt.%. The calcined clay was sourced from Argeco, France obtained by flash calcination of raw clay. The kaolinite content of raw clay was 55 wt.% which classified as low-grade clay. The limestone (branded as Omyacarb) was supplied by Oyma Australia Pty. Ltd.

The third low-carbon binder is a geopolymer binder. The precursor is composed of calcined clay and Ground Granulated Blast-Furnace slag (GGBFS). GGBFS was produced by Australian Steel Mill Services (ASMS), Port Kembla, New South Wales, Australia. The chemical composition of hydrated lime, calcined clay, limestone and GGBFS, determined by X-ray fluorescence (XRF), is presented in Table 1. The activator solution for the geopolymer mix contained sodium hydroxide pellets and sodium silicate solution. The specifications of NaOH pellets included a specific gravity of 2.1, a molecular weight of 40 and a purity of 98%. The sodium silicate solution consisted of 9.1 wt.% Na_2O, 28.9 wt.% SiO_2 and 61.1 wt.% H_2O with the molar ratio SiO_2: $Na_2O = 3.16–3.26$.

2.3 Mix design and batching procedure

This study investigates four hempcretes with different binders: hempcrete HL-Ref is the reference

Table 1 Chemical composition of hydrated lime, calcined clay, limestone and GGBFS

Chemical composition (wt.%)	Hydrated lime	Calcined clay	Limestone	GGBFS
SiO_2	1.3	70.4	1.1	31.5
Al_2O_3	0.5	22.3	0.2	12.2
Fe_2O_3	0.3	2.3	0.2	1.1
CaO	71.8	0.5	54.8	44.5
MgO	0.8	0.2	1.5	4.6
Na_2O	–	0.1	–	0.2
K_2O	–	0.2	–	0.3
TiO_2	0.1	1.1	–	1.0
SO_3	–	–	–	3.2
Loss on ignition (LOI)	25.5	1.8	43.1	0.8

hempcrete with only hydrated lime. 100% hydrated lime binder is the conventional binder to fabricate hempcrete in Australia. Hempcrete HL–CC is the first low carbon binder hempcrete considered with 50 wt.% of the hydrated lime being replaced by calcined clay. Hempcrete HL–CC–LS is the second low carbon binder hempcrete with 50 wt.% of the hydrated lime being replaced by a blend of limestone and calcined clay (calcined clay to limestone ratio of 2). Hempcrete Geo-CC uses a geopolymer binder with 70 wt.% calcined clay and 30 wt.% Ground Granulated Blast furnace Slag (GGBFS) being activated using the sodium hydroxide and sodium silicate solution [30].

Table 2 represents the density of the raw powder materials used for the four hempcretes investigated, namely hydrated lime, limestone powder, calcined clay and GGBFS, obtained using an Anton Paar Ultrapyc 5000. It is observed that the density for GGBFS is significantly higher than the density of the other materials.

The mix design of all hydrated lime-based hempcretes was 1:1.8:1:2 hurds, binder, sand and water, except for geopolymer-based hempcrete. The HL-Ref mix design was formulated similarly to the hempcrete mix design used in the Australian industry. As mentioned above, the main objective is to reduce the content of the carbon intensive hydrated lime in hempcrete. 50 wt.% hydrated lime was substituted in HL–CC and HL–CC–LS mixes, while mix Geo-CC is hydrated lime free. Calcined clay replaced 50 wt.% of hydrated lime in mix HL–CC. In the mix HL–CC–LS, calcined clay and limestone replaced 33.3 wt.% and 16.7 wt.% of binder content respectively. The mix design of all geopolymer-based hempcretes (Geo-CC) was 1:1.8:1:0.15:0.65:1.1 for hurds, binder, sand, sodium hydroxide pellets, sodium silicate solution and water [28].

Table 2 Density of the raw powder materials used in hempcrete (kg/m^3)

Raw materials	Average density	Standard deviation
GGBFS	3022.3	1.3
Limestone	2545.5	17.0
Hydrated lime	2503.0	0.6
Calcined clay	2715.2	1.27

For all mixes, Sydney sand was used as the fine aggregate. Sydney sand relative density and water absorption values were 2876 kg/m^3 and 3.5% respectively. The gradation of Sydney sand is shown in Fig. 1. For the Geo-CC mix, the activator solution containing NaOH pellets, sodium silicate solutions and free water were prepared 24 h prior to mixing. The hempcrete was mixed in a 70L electric pan mixer. Hemp hurds absorb a large amount of water during mixing, which affects the workability of the hempcrete mixture. The high water absorption of hurds requires additional water to ensure proper hydration of the lime binder and to achieve a homogeneous mix. Therefore, a specific mixing procedure was followed to ensure sufficient free water for the mixing and hydration process [22]. Firstly, the hemp hurds were placed in the mixer and mixed for 30 s. Secondly, water was added to achieve Saturated Surface Dry (SSD) condition, which was calculated based on the initial water content (INC) in hurds, and mixed for 1 min. This step ensured that the hemp hurds did not absorb any of the free water which is required for the binder reaction process.

Lastly, both the binder and free water (or activator solution) were evenly distributed over the wet hemp and mixed for 2 min. The mixing procedure was followed the current engineering practice. Cylindrical and prismatic specimens were fabricated from the fresh hempcrete mixture. The specimens were compacted into 100 mm diameter cylinders using a 2.7 kg compacting hammer generating an approximate compacting energy of 38 kJ/m^3. The specimens were filled by 3 compacted layers. The hammer was dropped 5 times per layer for cylinders and 13 times per layer for prisms (100 × 100 × 400 mm) to obtain the same compact energy. All specimens were demoulded after 24 h and stored in a controlled room at a temperature of 23 ± 2 °C and relative humidity (RH) of 55 ± 3% until 28 days.

3 Experimental programs

3.1 Compressive strength and bulk density

The compressive strength test was performed using 100 mm diameter cylinder specimens with 200 mm

height after 28 days, which is widely utilised to measure the compressive strength of the conventional concretes. A clear different in reaction products between different binders can be observed at 28 days in conventional concretes [32, 36]. An example of cylinders from the different mix design is shown in Fig. 3. For all the testings, 3 samples were tested in each setting and iterations, and an average is reported. The compression tests were conducted on a universal testing machine in displacement control at a rate of 3 mm/min up to failure. A thin rubber sheet and polyethylene packing foam were added between the cylindrical samples and the press plates to ensure a smooth contact between the cylindrical sample and the press plates as well as an even distribution of the load across the cylinder surface. The bulk density was calculated by the measuring dimensions and weight the cylindrical samples [37].

3.2 Sound absorption and airflow resistivity

Hempcrete is a porous structure with interconnected pores which facilitates sound wave penetration, converting sound energy into heat through friction and attenuating sound through various mechanisms, such as viscous dissipation, thermoelastic damping, resonance and mechanical damping [38–40]. The sound absorption efficiency is influenced by material thickness, density, porosity, structural composition, and airflow resistance. While more and larger pores can enhance sound absorption, they might compromise the material's structural integrity. The study in this section focuses on two key metrics for porous sound absorbers: the normal incidence sound absorption coefficient and airflow resistivity. The normal incidence sound absorption coefficient refers to the proportion of sound energy absorbed when sound waves perpendicularly strike the material's surface. This coefficient is between 0 and 1, where a higher value signifies better sound absorption. Airflow resistivity is a fundamental parameter governing the sound absorption behaviour of different materials. It is defined as the ratio between the pressure drop and the flow velocity through a layer of material of unit thickness and indicates air permeability through the material [39, 40]. The higher the airflow resistivity, the less air permeability, resulting in reduced sound absorption due to fewer sound waves entering the material. However, smaller airflow resistivity lessens the transformation efficiency from sound energy to thermal energy. Therefore, an optimal airflow resistivity exists to maximize sound absorption efficiency [39, 40].

The sound absorption measurements for the frequency range of 50–1600 Hz were performed using a two-microphone impedance tube (Brüel & Kjær Type

Fig. 3 Hempcrete cylinders from reference mix HL-Ref (left) and mixes with calcined clay (middle and right)

4206) based on the transfer-function method by ISO 10534-2 standard [41]. The airflow resistivity measurements were performed using the same equipment following the test method in [42], with additional measurements of each sample backed by a 100 mm thick air cavity. Hempcrete samples with a thickness of 50 mm were prepared to fit the 100 mm internal diameter of the impedance tube. These samples were cast using 3D-printed cylindrical plastic moulds with one layer of compaction and subsequently stored in a controlled environment for 28 days prior to testing. For each specimen type, three individual samples were created. The sound absorption properties of the sample were measured twice: initially after 28 days of curing period (28D specimens), and subsequently after 332 days of curing period (332D specimens). Additionally, the flow resistivity of the samples was also determined after 332 days of curing period (332D). By measuring both sound absorption and airflow resistivity, it was possible to estimate the optimal airflow resistivity for each specimen. This allowed for a more accurate comparison of sound absorption across different specimens, minimizing bias caused by significant differences in airflow resistivity. Detailed information about the impedance tube can be found in Fig. 4, while the experimental results and analysis are presented in Sect. 4.2.

3.3 Thermal conductivity

The thermal characteristics are measured using a Hot Disc system using the transient plane source approach [13]. In comparison to all other existing measurement methods such as calorimeter, the Hot Disc method is quite flexible and offers significant advantages, making it appropriate for a range of applications. 100 mm diameter and 50 mm height hempcrete disc samples were used for thermal conductivity. The thermal conductivity was tested after 28 days of curing in the air-conditioned lab, with consistent ambient temperature of 20 ± 1 °C and humidity of $55 \pm 5\%$. Five replicated for each set of sample group was tested. The top and bottom surfaces were flattened by compaction, to achieve a flat and smooth surface ideal for the test. In the tests, two cut surfaces were used to form a sandwich structure with the sensor in the middle. The hot disk sensor diameter is 60 mm, significantly larger than the average hemp particle dimension, thus the measurement is considered as a homogeneous response. The samples are extracted at positions away from the top and bottom surfaces, where preferable fibre orientation could be relevant. Therefore, heterogeneity between the top and bottom parts could be minimised. The thermal conductivity was measured with the thermal power ranging from 100 to 250 mW and measuring duration of 640 s.

3.4 Hempcrete surface bond strength—Adhesion test

The surface bond strength was tested using the pull-out adhesion tester (Positest AT) on the surface of hempcrete prisms with a dimension of $100 \times 100 \times 400$ mm after 28 days of curing. A hydraulic pump in the adhesion tester was used to pull a dolly attached to the surface of the hempcrete specimen and the failure force was recorded. The test

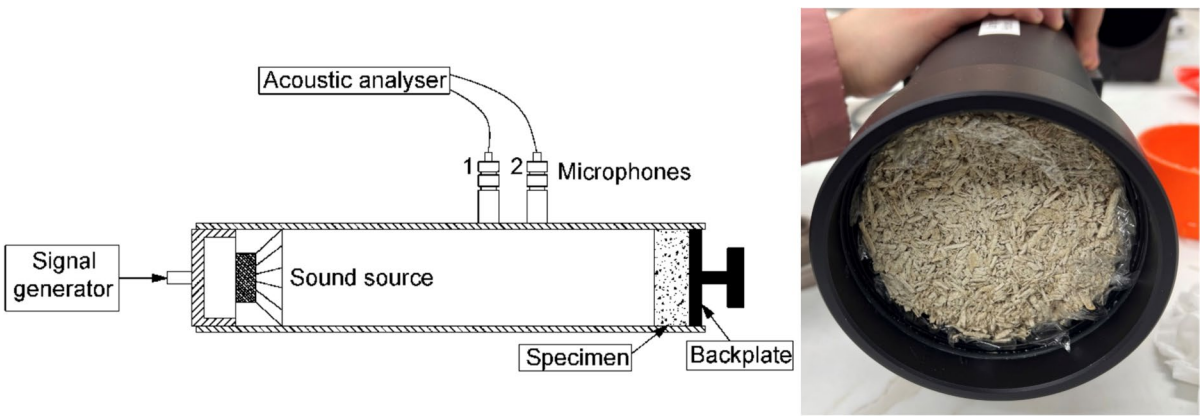

Fig. 4 Details of the impedance tube (left) and an example of hempcrete sample inside the impedance tube (right)

is used to evaluate the bond strength of hempcrete surface, ensuring that the hempcrete particles do not fall off during usage. The dolly with 50 mm diameter was glued with two-part epoxy to the lateral side of hempcrete specimens 24 h prior to the adhesion test. An example of adhesion test is shown in Fig. 5.

3.5 Crystalline phases by X-ray diffraction (XRD)

Paste cube specimens (50×50 mm) of HL-Ref, HL–CC and HL–CC–LS mixes were prepared based on the mix design details in Sect. 2.3 without hemp hurds and Sydney sand. The paste specimens were demoulded after 24 h of casting and cured in the controlled room. After 28 days, the paste was ground to pass 75 µm sieve size. The XRD measurement was carried out by a Bruker D8 Discover diffractometer using Cu-Kα radiation (wavelength of 0.154 nm) operated at 45 kV and 40 mA together with a step size of 0.013° 2θ and a sample spinner at UTS Microstructural Analysis Unit (MAU). The crystalline phases detected from XRD analysis were used to elaborate the hempcrete performance with different mix designs.

4 Results and discussion

4.1 Compressive strength and bulk density

The compressive strength as the average of hempcrete cylinders at 28 days is presented in Fig. 6. The reference mix HL-Ref exhibited a compressive strength of 0.16 MPa, which is similar to the compressive strength of HL–CC hempcrete containing 50 wt.% hydrated lime and 50 wt.% calcined clay. This indicates that replacing 50 wt.% of hydrated lime using calcined clay in HL–CC mix did not negatively affect the compressive strength. Substituting 50 wt.% of hydrated lime by a combination of calcined clay and limestone in HL–CC–LS mix led to an increase in the compressive strength of about 60% at 0.26 MPa compared to the reference hempcrete, highlighting the synergy benefits of limestone and calcined clay in lime-based system. Noticeably, the geopolymer hempcrete (Geo-CC) exhibited the highest 28-day compressive strength of 0.65 MPa, which is approximately four times higher than that of the HL-Ref. The high compressive strength of Geo-CC mix also demonstrates the suitability of geopolymer binder for hempcrete applications. Narattha et al. [26] reported the utilisation of fly ash geopolymer to produce hemp

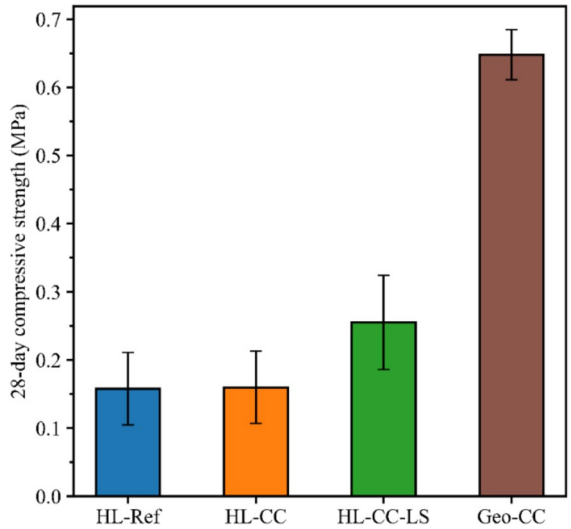

Fig. 6. 28-day compressive strength of hempcrete

Fig. 5 Adhesion tester details: **a** The hydraulic pump with digital screen. **b** A dolly after failure

shiv lightweight aggregate. However, the chemical treatment with a complex mineraliser of $AlCl_3$ and KOH was required [26]. In contrast, Geo-CC hempcrete in this study does not require any chemical treatment. Overall, the compressive strength results of the four mixes in this study fell within the range reported in previous studies for bio-based composites that used hemp, wood, sunflower pith, corn (maize), rice straw, or rice husk as coarse aggregate [16, 43–49]. Moreover, the compressive strength values in this study were consistent with results of the previous study of the authors [37], indicating negligible effect of the water absorption properties of hemp hurds on the compressive strength. This can be attributed to the mixing procedure as described in Sect. 2.3 that eliminates the influence of hemp hurds water absorption. Traditional concrete, depending on its mix design, typically exhibits compressive strengths ranging from 20 to 40 MPa for most applications. In contrast, Geo-CC hempcrete compressive strength is extremely lower (less than 1 MPa) due to the low density of hemp hurds and its low binder content. Hempcrete is a non-bearing material. Therefore, high compressive strength similar to traditional concrete is not required. Hempcrete offers excellent thermal insulation, carbon sequestration, and sustainability benefits compared to traditional concrete. Specifically, Yadav and Saini [50] highlighted that while hempcrete cannot match the compressive strength of traditional concrete, it outperforms traditional concrete in terms of environmental impact and energy efficiency.

Figure 7 shows the bulk density results from 7 to 28 days of the hempcrete specimens cured in the control room. The bulk density exhibits a reduction trend as the specimens were drying during the curing period. The 50 wt.% replacement of hydrated lime by calcined clay in HL–CC hempcrete resulted in the lowset bulk density over the test duration. HL–CC hempcrete bulk density was at around 530 kg/m^3 at 7 days and then stabilised at 475 kg/m^3 from 14 to 28 days. HL-Ref showed a consistent reduction in bulk density from 625 kg/m^3 at day 7 to 530 kg/m^3 at day 28. HL–CC–LS hempcrete with 50 wt.% calcined clay and limestone exhibited a comparable bulk density to the HL-Ref hempcrete with 610 kg/m^3 and 545 kg/m^3 at day 7 and day 28 respectively. The maximum bulk density belongs to the geopolymer hempcrete CC-Geo which also achieved the highest 28 days compressive strength. This high bulk density

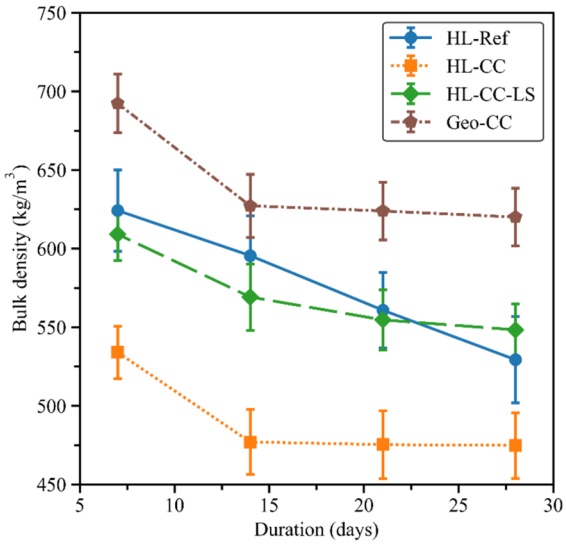

Fig. 7 Results of bulk density from 7 to 28 days

is due to the high density of GGBFS compared to hydrated lime, calcined clay and limestone powder (Table 2) and also the higher density of the geopolymer activator compared to water. The bulk density of CC-Geo hempcrete reduced from 690 kg/m^3 at 7 days to 620 kg/m^3 at 28 days. Overall, the increase in bulk density correlates could lead to the increase in hempcrete compressive strength. In addition, the bulk densities measured in this study are consistent with the results from previous studies on hempcrete [16, 43, 51]. The bulk density values in this study are slightly higher than the values reported in the previous study of the authors [37] due to the addition of sand. The low bulk density of hempcrete compared to traditional concrete negatively impacts the mechanical properties. However, it leads to excellent acoustic performance, thermal insulation, and sustainability benefits compared to traditional concrete as a result of its low binder content.

4.2 Sound absorption and airflow resistivity

Figure 8 presents the sound absorption coefficients determined by the impedance tube test, conducted across the frequency range of 50–1600 Hz on 28D and 332D. These coefficients represent the average values obtained from testing three samples per specimen. In general, the sound absorption coefficients of hempcrete were significantly higher than

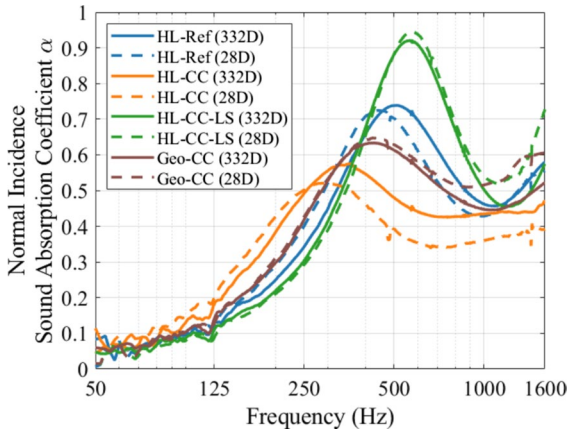

Fig. 8 Normal incidence sound absorption coefficients measured on 28D (shown with dashed curves) and later on 332D (shown with solid curves)

that of normal concretes [52]. Figure 8 shows that HL–CC–LS had a peak sound absorption coefficient of 0.94 in 28D and 0.92 in 332D, around 572 Hz. In contrast, HL–CC has the highest sound absorption at frequencies below 315 Hz. A comparative analysis of the data from 28 to 332D indicates that HL–CC–LS and Geo-CC experienced degradation in sound absorption at mid to high frequencies, particularly around the trough succeeding the resonance peak, while the absorption at low frequencies remained unchanged. Meanwhile, HL-Ref and HL–CC shifted their absorption curves towards higher frequencies, coupled with enhanced absorption at the resonance peak. However, they showed diminished performance at frequencies below the original resonance peak. Compared to the previous research [13], the samples analysed in this study exhibit a higher bulk density. This increase in density is a contributing factor to the resonance observed at lower frequencies, aligning with the observations reported in [13].

To quantify the sound absorption of the sample using a single-number rating akin to the Noise Reduction Coefficient (NRC) [53], we computed the average sound absorption as follows:

$$\alpha_{\mathrm{Avg}} = \left(\alpha_{\mathrm{Oct},250} + \alpha_{\mathrm{Oct},500} + \alpha_{\mathrm{Oct},1000}\right)/3 \tag{1}$$

where $\alpha_{\mathrm{Oct},f_c}$ is the sound absorption value for three octave bands centred at 250 Hz, 500 Hz, and 1000 Hz, respectively. This is calculated by

$$\alpha_{\mathrm{Oct},f_c} = \frac{\sum_{f=f_c^{\mathrm{l}}}^{f_c^{\mathrm{u}}} \alpha(f)}{f_c^{\mathrm{u}} - f_c^{\mathrm{l}} + 1}, \tag{2}$$

with the upper limit frequency $f_c^{\mathrm{u}} = \mathrm{round}\left(\sqrt{2} f_c\right)$ and the lower limit frequency $f_c^{\mathrm{l}} = \mathrm{round}\left(f_c/\sqrt{2}\right)$, for each octave band centered at $f_c = 250, 500,$ or 1000 Hz. Here, $\alpha(f)$ denotes the sound absorption coefficients at individual frequencies within the octave band. Results indicate that HL–CC–LS has the best average sound absorption α_{Avg}, though with the worst low-frequency performance as indicated by $\alpha_{\mathrm{Oct},250}$.

Table 3 also presents the airflow resistivity results for each specimen, measured on 332D specimens. There is a notable disparity in airflow resistivity among the specimens. To facilitate a more accurate interpretation of the sound absorption results and mitigate bias caused by these differences, the optimal airflow resistivity for each specimen was estimated to gauge their maximum potential sound absorption efficiency [39, 40]. This estimation is shown in the final column of Table 3 and elaborated upon in Fig. 9, calculated as follows. First, the Delaney and Bazley formulation was utilised [54] to interpolate the absorption coefficient values across varying flow resistances. The interpolation is presented as follows:

$$\widetilde{\alpha}(\sigma, f) = \frac{\alpha_{\mathrm{DB}}(\sigma, f)}{\alpha_{\mathrm{DB}}\left(\sigma_0, f\right)} \bullet \alpha\left(\sigma_0, f\right) \tag{3}$$

where $\alpha_{\mathrm{DB}}(\sigma, f)$ represents sound absorption derived from the Delaney and Bazley formulation, detailed in Sect. 6.5.1 in [39] using a corresponding Matlab script [55]. Next, the estimated average sound absorption was calculated as follows:

$$\widetilde{\alpha}_{\mathrm{Avg}}(\sigma) = \left[\widetilde{\alpha}_{\mathrm{Oct},250}(\sigma) + \widetilde{\alpha}_{\mathrm{Oct},500}(\sigma) + \widetilde{\alpha}_{\mathrm{Oct},1000}(\sigma)\right]/3 \tag{4}$$

where 'tilde' denotes the estimated value. Thus, the optimal airflow resistivity that yields the maximum average sound absorption is:

$$\sigma_{\mathrm{opt}} = \max_{\sigma}\left[\widetilde{\alpha}_{\mathrm{Avg}}(\sigma)\right] \tag{5}$$

and the estimated maximum average sound absorption is:

Table 3 Comparative analysis of sound absorption in three octave bands (250 Hz, 500 Hz, and 1000 Hz) and average absorption of 28D and 332D specimens, along with flow resistivity measured and estimated average absorption with optimal flow resistivity on 332D specimens

Hempcrete specimens	Absorption 250 Hz $\alpha_{Oct,250}$ 28D/332D	Absorption 500 Hz $\alpha_{Oct,500}$ 28D/332D	Absorption 1000 Hz $\alpha_{Oct,1000}$ 28D/332D	Avg. absorption α_{Avg} 28D/332D	Flow resistivityσ (N/m^4) 332D	Opt. Avg Absorption $\tilde{\alpha}_{Avg,opt}$ 332D
HL-Ref	0.44/0.38	0.65/0.68	0.47/0.49	0.52/0.52	27,975	0.52
HL–CC	0.49/0.49	0.39/0.48	0.36/0.43	0.41/0.47	43,061	0.49
HL–CC–LS	0.33/0.35	0.83/0.82	0.59/0.53	0.58/0.57	12,819	0.61
Geo-CC	0.45/0.44	0.60/0.59	0.54/0.46	0.53/0.50	40,290	0.52

$$\tilde{\alpha}_{\text{Avg, opt}} = \tilde{\alpha}_{\text{Avg}}\left(\sigma_{\text{opt}}\right). \quad (6)$$

It's important to note that the Delaney and Bazley formulation is applicable only within a specific frequency range, approximately 207 Hz–20 kHz for flow resistivity of 25,000N/m^4 [39], and requires modification at low frequencies [56]. Considering the relatively low absorption at these frequencies and the objective of optimizing average absorption across bands, the Delaney and Bazley model, being a macroscopic empirical model, is ideally suited for determining the optimum airflow resistivity in the hempcrete, which are porous materials with irregular internal structures. As shown in Fig. 9, the optimal airflow resistivity values are similar among the specimens compared. When using the optimal airflow resistivity, the estimated overall sound absorption performance is observed as HL–CC–LS > HL-Ref ≈ Geo-CC > HL–CC.

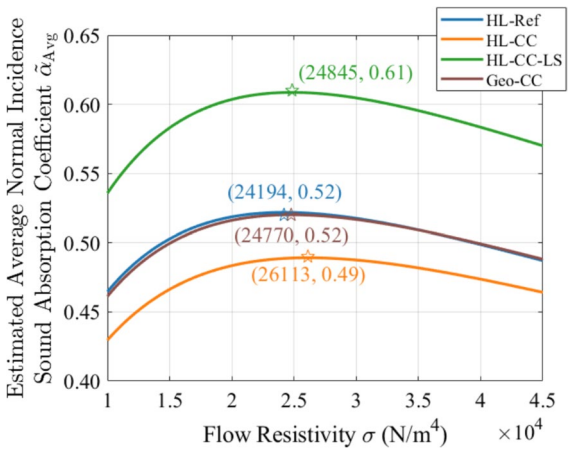

Fig. 9 Estimated average normal incidence sound absorption coefficient across different airflow resistivities. A star symbol indicates the optimal airflow resistivity and its associated peak sound absorption

As hempcrete is a porous bio-based concrete, its acoustic properties are highly influenced by its complex porous structure, which is affected by various factors, such as the manufacturing process, the binder composition and mix formulation. It is generally reported that the absorption coefficient of hempcrete samples should range between 0.3 and 0.9 [57]. All the absorption coefficients in Table 3 of the hempcrete tested are within this range. In addition, the sound absorption coefficients of the hempcrete specimens in this study are comparable to those of conventional and advanced insulation materials used in the building industry, such as rock wool, polyurethane, aerogel, and nano-insulation materials [58]. However, significant differences can be noticed depending on the binder composition in Table 3. In general, the variation trend of α_{Avg} and $\tilde{\alpha}_{Avg,opt}$ is similar between the different mixes. For convenience, the values presented below are based on the measurements conducted on 28D specimens, immediately following the 28-day curing period. Compared to the reference mix (HL-Ref), the replacement of 50 wt.% hydrated lime by only calcined clay (HL–CC) negatively affected the acoustic performance, leading to a significant reduction of the resonance peak from 0.72 to 0.52 with also a significant shift in the resonance frequency from 446 to 286 Hz, shown in Fig. 8. A reduction of α_{Avg} value from 0.52 in HL-Ref to 0.41 in HL–CC hempcrete was observed. Hempcrete HL–CC is also the hempcrete achieving the lowest 28 days bulk density (Fig. 7). However, blending calcined clay with limestone in HL–CC–LS hempcrete led to a large increase in the sound absorption coefficient

compared to the reference mix from 0.72 to 0.94 for the resonance peak, and from 0.52 to 0.58 for α_{Avg}. As already observed for compressive strength results in Fig. 6, for the same hydrated lime replacement rate of 50 wt.% incorporating limestone calcined clay system leads to a significant performance improvement that cannot be achieved by using only calcined clay. The resonance frequency also slightly shifted from 446 to 572 Hz. The reasons for better acoustics performance of HL–CC–LS will be discussed in Sect. 4.6. The performance of the geopolymer hempcrete (Geo-CC) was similar to the reference mix (HL-Ref) in terms of α_{Avg}, despite having a significantly higher 28-day bulk density than the reference mix (Fig. 7). The peak sound absorption at the resonance frequency is lower than the values reported in the previous study of the authors [37], which can be attributed to the higher bulk density due to the addition of sand. Moreover, the sound absorption coefficient of hempcrete in this study was within the range of other natural building insulation materials such as bamboo fibres, rice husk and bagasse [58]. The findings from the measurements taken on 28D specimens have been cross-validated with those from 332D, and the estimated sound absorption at the optimal airflow resistivity. While the precise sound absorption values vary with the test dates and airflow resistivity, the comparative trend among the specimens remains consistent: HL–CC–LS > HL-Ref ≈ Geo-CC > HL–CC in terms of overall sound absorption performance.

4.3 Thermal conductivity

Figure 10 presents the thermal properties of hempcrete mixes at 28 days after curing, including thermal conductivity and probing depth. The observed trends in these properties exhibit a similar pattern, which is consistent with their inherent correlation. The thermal conductivity was significantly lower than that of normal weight concretes and bricks [59, 60]. Among the tested hempcrete, the geopolymer hempcrete Geo-CC stands out for its superior thermal performance, evidenced by its lowest thermal conductivity of 0.085 W/mK. The lower thermal conductivity of the geopolymer hempcrete compared to the other hempcretes is unexpected as hempcrete thermal conductivity is usually increasing as its density is increasing [61]. This could be due to the thermal conductivity of the binder itself. Indeed, the thermal conductivity of calcined clay based geopolymer paste was investigated by Van Riessen [62], ranging from 0.55 to 0.65 W/mK, values being considered significantly lower than that of traditional lime-based binder pastes. Another reason could be the high delignification of hemp hurds due to the high pH of the activator which can also lead to a reduction in thermal conductivity of hempcrete [60]. Further investigations will have to be carried out in the future to clarify the role of both binder properties and hemp hurds delignification on the thermal conductivity of hempcrete. In contrast, the hempcrete HL–CC demonstrated the least favourable results, with the highest measured thermal conductivity of 0.151 W/mK. Enhancements in thermal conductivity were also noted with the addition of limestone to the binder (HL–CC–LS), which significantly improved the performance of the calcined clay and hydrated lime blend system (HL–CC). Notably, the thermal conductivity of the HL–CC–LS mixture, approximately 0.1 W/m K, was about 15–40% lower than that of other bio-based composites with similar densities that use wood, sunflower pith, or corn (maize) as aggregates [46–48]. The thermal conductivity of the HL–CC–LS mixture was also comparable to that of bio-based composites made with a 50% rice straw and 50% rice husk aggregate blend [49]. The effect of the combination of calcined clay and limestone in hempcrete performance is discussed in Sects. 4.5 and 4.6. Moreover, this adjustment resulted in lower thermal conductivity compared to the reference hempcrete, mirroring the sound absorption improvements observed. The thermal conductivity of HL-Ref aligns with the results reported in the previous study of the

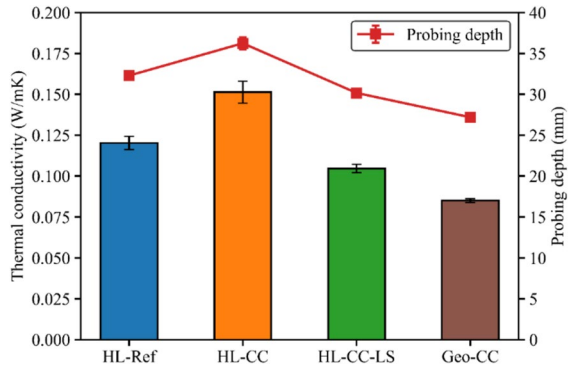

Fig. 10 Thermal conductivity and probing depth of hempcrete specimens after 28 days of curing

authors [37]. When comparing the water absorption of hemp hurds and the presence of sand in this study and the previous study [37], low water absorption and sand content have a minimal impact on thermal performance.

4.4 Hempcrete surface bond strength

The hempcrete surface bond strength results after 28 days of curing assessed by pull-out adhesion test is shown in Table 4. Each test result was the average of three adhesion tests. The reference mix HL-Ref exhibited the lowest bonding capacity with the lowest test result of 0.15 MPa whilst Geo-CC hempcrete obtained the highest strength at 0.36 MPa. HL–CC achieved 0.18 MPa. The addition of limestone in HL–CC–LS mix improved the performance by increasing the bonding capacity to 0.21 MPa which was approximately 15% higher than HL–CC hempcrete. Overall, the surface bond strength was well-correlated with the compressive strength results shown in Fig. 6. Higher surface bond strength between the hemp shiv and the binder improves the material's ability to withstand compressive loads. This is because a strong bond ensures effective load transfer and minimizes stress concentrations at the interface. The high surface bond strength also indicates a strong interfacial transition zone (ITZ) between the hemp hurds and binders. A better ITZ can reduce microcracking and enhance the hempcrete's overall structural integrity.

4.5 Crystalline phases by XRD analysis

The XRD patterns of HL-Ref, HL–CC and HL–CC–LS pastes after 28 days of curing are exhibited in Fig. 11. Geo-CC mix results are not presented as the XRD analysis, including N–A–S–H, C–(A)–S–H and C–N–(A)–S–H, was reported in the previous study of the authors [30]. The XRD patterns of the reference mix HL-Ref mainly shows the Portlandite ($Ca(OH)_2$) with the highest peak at 34.1° 2θ. In addition, the peak of calcite ($CaCO_3$) was observed at 29.4° 2θ demonstrating the ongoing carbonation process in the HL-Ref paste. The considerably lower intensity of calcite peak comparing to Portlandite peaks in the XRD pattern indicated the slow carbonation process, leading to the low compressive strength of HL-Ref hempcrete in Fig. 6. Small peaks of dicalcium silicate (C_2S) were detected between 32–33° 2θ which is consistent with the small amount of SiO_2 in the chemical composition presented in Table 1.

In contrast, the presence of calcined clay and limestone significantly modified the crystalline phases as well as reaction mechanisms of HL–CC and HL–CC–LS pastes presented in Fig. 11. In the HL–CC paste, the highest peak belonged to Quartz at 26.6° 2θ, which was the main inert crystalline phase of calcined clay [30]. The intensity of Portlandite peaks in HL–CC paste was considerably lower than the Portlandite peaks in HL-Ref paste. In addition, the peak at 29.4° 2θ of HL–CC was significantly higher than that of HL-Ref. This can be attributed to the pozzolanic reaction between amorphous phases of calcined clay and Portlandite to form calcium–silicate–hydrates (C–S–H), as also detected at 29.4° 2θ [36]. Small peak of zeolite (C–A–S–H) is shown at around 24° 2θ, which indicates the reaction between reactive Al_2O_3 and SiO_2 from calcined clay with $Ca(OH)_2$ from hydrated lime. The formation of hemicarbonaluminate ($Ca_4Al_2(CO_3)_{0.5}(OH)_{13}\cdot 5.5H_2O$) and monocarboalumniate ($Ca_4Al_2(CO_3)(OH)_{12}\cdot 5H_2O$) was observed at main peaks of 10.8° and 11.7° 2θ in HL–CC paste respectively. The presence of these carboaluminate phases can be explained by the reaction of calcined clay and limited calcite formed from the carbonation progress of Portlandite in the hydrated lime. In summary, regarding the mechanical strength, the replacement of 50 wt.% hydrated lime by calcined clay in HL–CC hempcrete can be compensated by the formation of C–S–H, C–A–S–H, hemi- and monocarboaluminate, demonstrating by the similar compressive strength at 28 days between HL-Ref and HL–CC hempcrete in Fig. 6.

In HL–CC–LS paste, the intensity of Portlandite peaks were slightly higher than in HL–CC paste. This can be attributed to the lower proportion of calcined clay in binder composition of HL–CC–LS

Table 4 Adhesion test results of hempcrete at 28 days

Hempcrete specimens	Pull-out adhesion test result (MPa)
HL-Ref	0.15 ± 0.04
HL–CC	0.18 ± 0.01
HL–CC–LS	0.21 ± 0.05
Geo-CC	0.36 ± 0.10

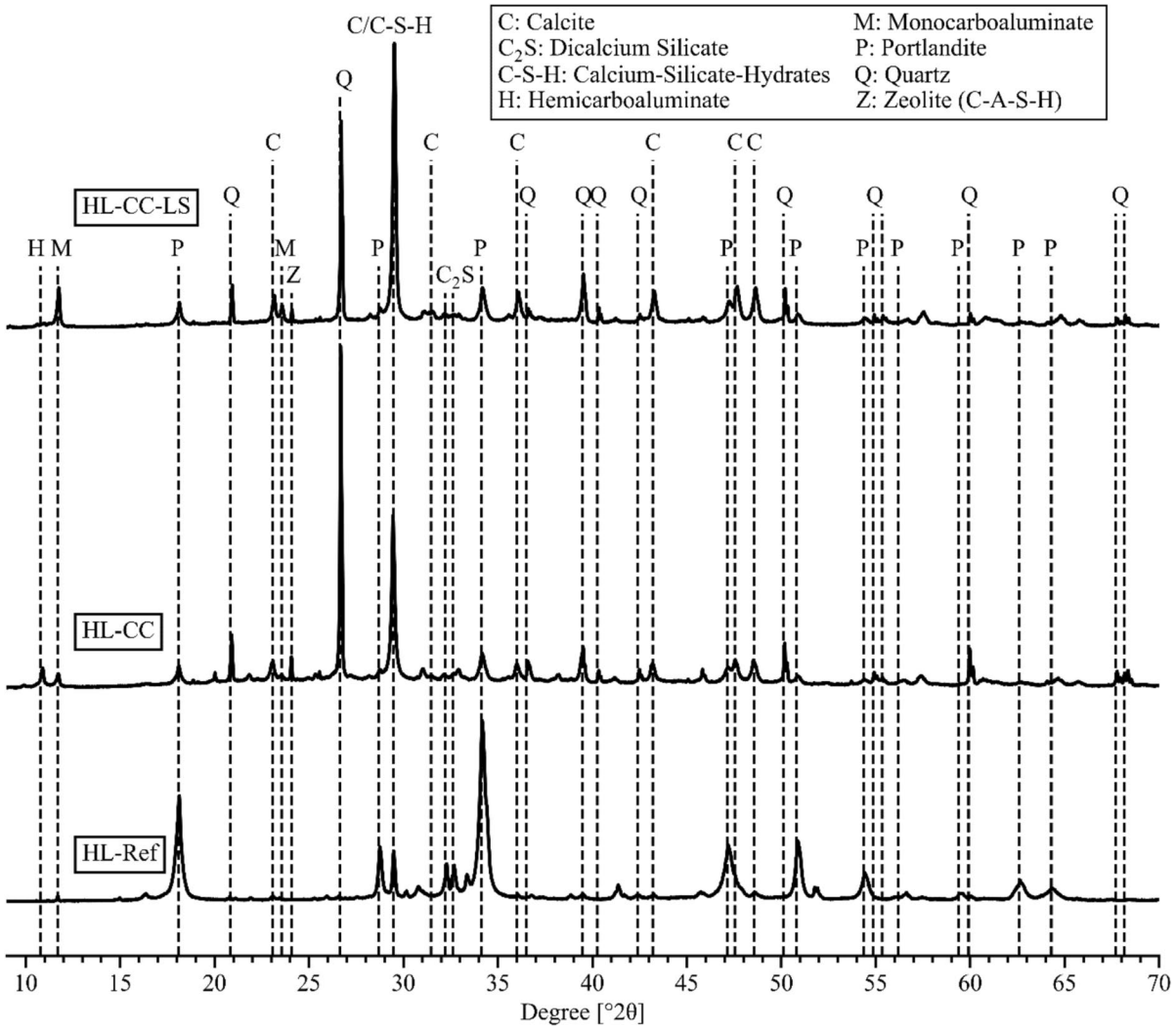

Fig. 11 XRD patterns of HL-Ref, HL–CC, and HL–CC–LS hempcrete at 28 days

in comparison to HL–CC mix, leading to a lower pozzolanic reactivity in HL–CC–LS. The peaks at 29.4° 2θ for calcite/C–S–H had the highest intensity among the three pastes due to the presence of limestone in the mixture. Noticeably, the monocarboaluminate phase exhibited the highest intensity whilst no hemicarboaluminate formation was observed in HL–CC–LS paste. In fact, the monocarboaluminate formation was favourable over hemicarboaluminate in the presence of excess calcite i.e., limestone [63], indicating the beneficial effects of limestone addition in the hydrated lime-based binder. The large amount of monocarboaluminate can contribute to the much better performance of HL–CC–LS hempcrete than the reference mix HL-Ref in terms of compressive strength, sound absorption, thermal conductivity, and particles bonding.

4.6 Discussion on multicriteria analysis in hempcrete performance

To provide a comprehensive assessment of the different hempcretes performance, Fig. 12 exhibits the multicriteria analysis of several properties including compressive strength, bulk density, average sound absorption α_{Avg}, thermal conductivity, and particles bonding capacity at 28 days. A unidimensional scale between 0 and 10 was utilised for each property. The

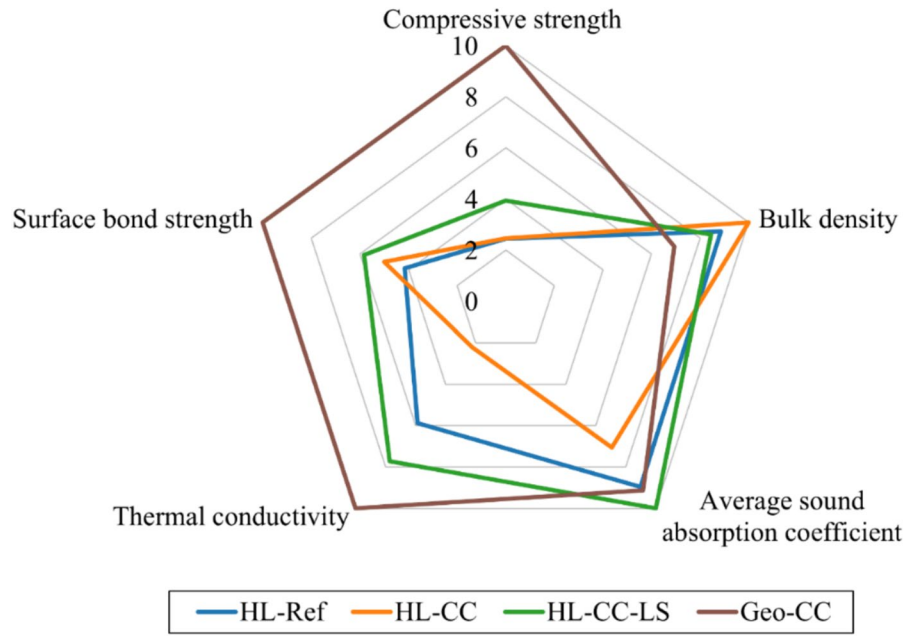

Fig. 12 Comparison of several properties of four hempcrete mixes in this study

highest performance in each property was normalised as 10 marks. In addition, the better performance definition was divided into two groups: higher value for compressive strength, average sound absorption coefficient, and surface bond strength while lower value for bulk density and thermal conductivity. To be specific, the higher value of compressive strength results in the better structural performance of hempcrete while higher sound absorption coefficient reduces the overall noise levels and improves the acoustic comfort of the building environment. The higher surface bond strength leads to better cohesion of hempcrete particles and better integrity of hempcrete structures. The lower bulk density results in less material consumption to satisfy structural requirements while lower thermal conductivity reduces the heat transmission in hempcrete. The Geo-CC hempcrete presented the best performance in terms of compressive strength, thermal conductivity, and particle bonding. This could be attributed to the formation of phases such as N–A–S–H, C–(A)–S–H and C–N–(A)–S–H leading to a better microstructure densification [30]. However, the usage of geopolymer binder results in the lower sound absorption coefficient compared to HL-Ref and HL–CC–LS and the highest bulk density among four mix designs. As a result, the Geo-CC hempcrete shows a potential to be utilised in applications where sound absorption capacity is not a crucial specification. Traditional precursors including fly ash and slag were considered as geopolymer precursors to produce hempcrete in previous studies [25, 26] but required hemp hurds chemical treatment. The results of Geo-CC hempcrete indicated a strong feasibility of using geopolymer as a low-carbon binder in hempcrete technology because the precursor of Geo-CC mix contains 70 wt.% low-grade calcined clay which has a global availability [27] without requiring any chemical treatment of hemp hurds. As geopolymer technology has been successfully used for precast concrete elements [64, 65], the Geo-CC hempcrete can be also an option for precast hempcrete bricks and panels.

HL–CC with 50 wt.% hydrated lime replaced only by calcined clay presents the lowest sound absorption and highest thermal conductivity but the best bulk density (lowest value). In addition, HL–CC achieved a comparable compressive strength and better particles bonding capacity than HL-Ref, which can be attributed to the formation of C–S–H, C–A–S–H, hemi- and monocarboaluminate phases.

Interestingly, HL–CC–LS hempcrete achieved a comparable bulk density to HL-Ref and outperforms HL-Ref hempcrete in all other properties (Fig. 12). These results show the advantages of incorporating limestone calcined clay into the hydrated lime binder significantly improve the performance of hydrated

lime hempcrete. Furthermore, the addition of limestone can improve the performance of calcined clay-hydrated lime binder (HL–CC hempcrete), leading to the better compressive strength, sound absorption, thermal conductivity, and particles bonding capacity of HL–CC–LS hempcrete. This highlights the significantly beneficial effects of limestone calcined clay system in hydrated lime binder to fabricate hempcrete. The remarkable formation of monocarboaluminate, which is a more stable phase than hemicarboaluminate, as observed in the XRD pattern (Fig. 11) can explain the outstanding performance of HL–CC–LS hempcrete. The presence of monocarboaluminate reduces the porosity [28, 66], along with limestone, being a filler material, helping in retaining a uniform pore network in HL–CC–LS binder for better performance. Moreover, limestone is the component with the lowest environmental impact, cost and energy usage compared to hydrated lime and calcined clay, as only a grinding process is required [29, 67]. The embodied carbon of original Portland cement (OPC), hydrated lime, calcined clay, GGBFS is 0.95, 1.20, 0.20, 0.02 kg CO_2e/kg materials respectively [29, 68]. Therefore, the addition of limestone can further enhance the sustainability of HL–CC–LS hempcrete. Overall, limestone calcined clay system with 50 wt.% replacement of hydrated lime can be a viable option for a sustainable hempcrete technology without incurring any significant technical difficulties. In addition, the long-term performance of hempcrete with these binders will be reported in a future study.

5 Conclusions

The study explored several low-carbon binders by using calcined clay, limestone and GGBFS to fabricate hempcrete. 50 wt.% hydrated lime was replaced by only calcined clay (HL–CC) or a combination of calcined clay and limestone (HL–CC–LS) in lime-based binder whilst 70 wt.% calcined clay and 30 wt.% GGBFS was used as the precursor for the geopolymer hempcrete (Geo-CC). Five properties were investigated: compressive strength, bulk density, sound adsorption coefficient, thermal conductivity, and surface bond strength. The main outcomes of this study can be summarised below:

- The geopolymer hempcrete Geo-CC achieved the maximum compressive strength, about four time higher than that of the reference hempcrete HL-Ref. The HL–CC mix showed a comparable compressive strength to HL-Ref whilst HL–CC–LS hempcrete achieved approximately 60% higher compressive strength than HL-Ref.
- The highest bulk density was also achieved by the Geo-CC hempcrete whist the lowest bulk density value belonged to the HL–CC hempcrete. Both Geo-CC and HL–CC mixes bulk density stabilised after 14 days of curing. HL-Ref and HL–CC–LS achieved comparable values and exhibited a consistent reduction trend in bulk density from 7 to 28 days due to drying.
- Despite Geo-CC hempcrete having the highest bulk density among the four mixes, its average sound absorption remains at least 0.5, comparable to HL-Ref and superior to HL–CC. The inclusion of limestone and calcined clay in the HL–CC–LS hempcrete mix achieves the best acoustic performance, with the peak sound absorption coefficient around 572 Hz, exceeding 0.9. This outcome is consistent across tests conducted after 28-day curing and 332-day curing, as well as for the average sound absorption estimated at optimal air flow resistivity.
- The geopolymer hempcrete Geo-CC achieved the lowest thermal conductivity. Results also showed that incorporating limestone into the calcined clay based binder greatly improved the thermal efficiency, underscoring the importance of material composition in optimizing the thermal properties of hempcrete.
- HL-Ref hempcrete showed the lowest surface bond strength and Geo-CC hempcrete exhibited the highest value. The bonding capacity values were well-correlated with the compressive strength results.
- From XRD patterns at 28 days, the presence of calcined clay in HL–CC hempcrete led to pozzolanic reactions with Portlandite from hydrated lime, forming C-S–H and small amounts of C-A-S–H. The formation of hemicarboaluminate and monocarboaluminate was also detected in HL–CC hempcrete due to the reaction between calcined clay and limited calcite from the carbonation of hydrated lime. Noticeably, a large amount of monocarboaluminate, which is more stable

phase than hemicarboaluminate, was observed in XRD patterns of HL–CC–LS due to the excess of $CaCO_3$ from limestone in the binder composition.
- The multicriteria analysis indicated that the Geo-CC hempcrete achieved the best performance in terms of compressive strength, surface bond strength and thermal conductivity, but also the lowest sound absorption coefficient. Thus, the Geo-CC hempcrete can be used in applications requiring high mechanical strength, low thermal conductivity, and only moderate sound absorption capacity.
- HL–CC–LS hempcrete presented a comparable bulk density to that of the reference hempcrete but superior performance in all other properties. This improvement in the performance could not be achieved by using only calcined clay (as in HL–CC hempcrete), highlighting the beneficial synergy between limestone and calcined clay in lime-based system. This can be attributed to the remarkable presence of monocarboaluminate in HL–CC–LS paste as determined by XRD analysis.

Acknowledgements This research was funded by the Australian Hemp Masonry Company Pty. Ltd. and the ARC Linkage project LP200200779 titled "Decarbonising built environments with hempcrete and green wall technology".

Authors contribution Siddharth Girish Nair: Writing—review and editing, Investigation, Data curation. Quang Dieu Nguyen: Writing—review and editing, Writing—original draft, Supervision, Visualization, Resources, Project administration, Methodology, Investigation, Formal analysis, Data curation, Conceptualization. Qiaoxi Zhu: Writing—review and editing, Writing—original draft, Investigation, Formal analysis, Data curation. Mahmoud Karimi: Writing—review and editing, Investigation. Yixiang Gan: Writing—review and editing, Investigation. Haiyi Zhong: Writing—review and editing, Investigation, Data curation. Arnaud Castel: Writing—review and editing, Supervision, Project administration, Investigation, Funding acquisition. Peter J. Irga: Writing—review and editing, Investigation. Cecilia Gravina da Rocha: Writing—review and editing, Investigation. Fraser R. Torpy: Writing—review and editing, Investigation. Sara Wilkinson: Writing—review and editing, Investigation. Danielle Moreau: Writing—review and editing, Investigation. Fabien Delhomme: Writing—review and editing, Investigation.

Funding Open Access funding enabled and organized by CAUL and its Member Institutions.

Data availability statements Data will be made available on reasonable request.

Declarations

Competing Interest The authors declare that they have no known competing financial interests or personal relationships that could have appeared to influence the work reported in this paper.

References

1. The Global Status Report for Buildings and Construction (Buildings-GSR), UN Environment Programme (2022)
2. Yu M, Wiedmann T, Crawford R, Tait C (2017) The carbon footprint of Australia's Construction Sector. Procedia Eng 180:211–220
3. Pickin J, Wardle C, O'Farrell K, Nyunt P, Donovan S, National Waste Report (2020) Department of Agriculture, Water and the Environment, 2020
4. Friedlingstein P, Houghton RA, Marland G, Hackler J, Boden TA, Conway TJ, Canadell JG, Raupach MR, Ciais P, Le Quéré C (2010) Update on CO_2 emissions. Nat Geosci 3:811–812
5. Andrew RM (2018) Global CO_2 emissions from cement production. Earth Syst Sci Data 10:195–217
6. Zabalza Bribián I, Valero Capilla A, Aranda Usón A (2011) Life cycle assessment of building materials: comparative analysis of energy and environmental impacts and evaluation of the eco-efficiency improvement potential. Build Environ 46:1133–1140
7. Ricciardi P, Belloni E, Cotana F (2014) Innovative panels with recycled materials: thermal and acoustic performance and Life Cycle Assessment. Appl Energy 134:150–162
8. Bousshine S, Ouakarrouch M, Bybi A, Laaroussi N, Garoum M, Tilioua A (2022) Acoustical and thermal characterization of sustainable materials derived from vegetable, agricultural, and animal fibers. Appl Acoust 187:108520
9. Zhang Z, Provis JL, Reid A, Wang H (2015) Mechanical, thermal insulation, thermal resistance and acoustic absorption properties of geopolymer foam concrete. Cement Concr Compos 62:97–105

10. Torres-Rivas A, Palumbo M, Haddad A, Cabeza LF, Jiménez L, Boer D (2018) Multi-objective optimisation of bio-based thermal insulation materials in building envelopes considering condensation risk. Appl Energy 224:602–614
11. Galimshina A, Moustapha M, Hollberg A, Padey P, Lasvaux S, Sudret B, Habert G (2022) Bio-based materials as a robust solution for building renovation: a case study. Appl Energy 316:119102
12. Ahmed ATMF, Islam MZ, Mahmud MS, Sarker ME, Islam MR (2022) Hemp as a potential raw material toward a sustainable world: a review. Heliyon 8:e08753
13. Delhomme F, Hajimohammadi A, Almeida A, Jiang C, Moreau D, Gan Y, Wang X, Castel A (2020) Physical properties of Australian hurd used as aggregate for hemp concrete. Mater Today Commun 24:100986
14. Barbhuiya S, Bhusan Das B (2022) A comprehensive review on the use of hemp in concrete. Constr Build Mater 341:127857
15. Florentin Y, Pearlmutter D, Givoni B, Gal E (2017) A life-cycle energy and carbon analysis of hemp-lime biocomposite building materials. Energy Build 156:293–305
16. Arnaud L, Gourlay E (2012) Experimental study of parameters influencing mechanical properties of hemp concretes. Constr Build Mater 28:50–56
17. Walker R, Pavia S (2014) Moisture transfer and thermal properties of hemp-lime concretes. Constr Build Mater 64:270–276
18. Fernea R, Manea DL, Plesa L, Iernuțan R, Dumitran M (2019) Acoustic and thermal properties of hemp-cement building materials. Procedia Manuf 32:208–215
19. Degrave-Lemeurs M, Glé P, Hellouin de Menibus A (2018) Acoustical properties of hemp concretes for buildings thermal insulation: application to clay and lime binders. Constr Build Mater 160:462–474
20. Arehart JH, Nelson WS, Srubar WV (2020) On the theoretical carbon storage and carbon sequestration potential of hempcrete. J Clean Prod 266:121846
21. Miller SA, Van Roijen E, Cunningham P, Kim A (2021) Opportunities and challenges for engineering construction materials as carbon sinks. RILEM Tech Lett 6:105–118
22. Nair SG, Nguyen QD, Zhu Q, Karimi M, Gan Y, Wang X, Castel A, Irga P, Rocha CGd, Torpy F, Wilkinson S,. Moreau D, Delhomme F (2025) Suitability of calcined clay and ground granulated blast furnace slag geopolymer binder for hempcrete applications. Built Environ Project Asset Manag (2025).
23. Barcelo L, Kline J, Walenta G, Gartner E (2013) Cement and carbon emissions. Mater Struct 47:1055–1065
24. Simoni M, Wilkes MD, Brown S, Provis JL, Kinoshita H, Hanein T (2022) Decarbonising the lime industry: State-of-the-art. Renew Sustain Energy Rev 168:112765
25. Ebrahim Z, Mastali M, Maguire M (2023) Toward sustainable lightweight durable bricks using alkali-activated hemp-based materials. Constr Build Mater 369:130609
26. Narattha C, Wattanasiriwech S, Wattanasiriwech D (2022) Thermal and mechanical characterization of fly ash geopolymer with aluminium chloride and potassium hydroxide treated hemp shiv lightweight aggregate. Constr Build Mater 331:127206
27. Snellings R, Almenares Reyes R, Hanein T, Irassar EF, Kanavaris F, Maier M, Marsh AT, Valentini L, Zunino F, Alujas Diaz A (2022) Paper of RILEM TC 282-CCL: mineralogical characterization methods for clay resources intended for use as supplementary cementitious material. Mater Struct 55:149
28. Nguyen QD, Khan MSH, Castel A (2018) Engineering properties of limestone calcined clay concrete. J Adv Concr Technol 16:343–357
29. Afroz S, Zhang Y, Nguyen QD, Kim T, Castel A (2023) Shrinkage of blended cement concrete with fly ash or limestone calcined clay. Mater Struct 56:15
30. Gomes SDC, Nguyen QD, Li W, Castel A (2023) Carbonation resistance of calcined clay-ground granulated blast furnace slag alkali-activated mortar. Constr Build Mater 393:131811
31. Nguyen QD, De Carvalho Gomes S, Alnahhal MF, Li W, Kim T, Castel A (2023) Testing geopolymer concrete performance in chloride environment. In: Jędrzejewska A, Kanavaris F, Azenha M, Benboudjema F, Schlicke D (eds) International RILEM conference on synergising expertise towards sustainability and robustness of cement-based materials and concrete structures. Springer Nature Switzerland, Cham, pp 1197–1203
32. Gomes SDC, Nguyen QD, Li W, Castel A (2024) Effects of mix composition on the mechanical, physical and durability properties of alkali-activated calcined clay/slag concrete cured under ambient condition. Constr Build Mater 453:139064
33. Gomes SDC, Pang Y, Nguyen QD, Li W, Vessalas K, Castel A (2025) The effect of calcined clay reactivity on the mechanical properties and chloride diffusion resistance of alkali-activated calcined clay-GGBFS concrete. J Build Eng 102:111996
34. Gomes SDC, Nguyen QD, Li W, Castel A (2025) Shrinkage and carbonation of alkali-activated calcined clay-ground granulated blast furnace slag (GGBFS) concrete. Cem Concr Res 194:107899
35. Amziane S, Collet F, Lawrence M, Magniont C, Picandet V, Sonebi M (2017) Recommendation of the RILEM TC 236-BBM: characterisation testing of hemp shiv to determine the initial water content, water absorption, dry density, particle size distribution and thermal conductivity. Mater Struct 50:167
36. Nguyen QD, Kim T, Castel A (2020) Mitigation of alkali-silica reaction by limestone calcined clay cement (LC3). Cem Concr Res 137:106176
37. Delhomme F, Castel A, Almeida A, Jiang C, Moreau D, Gan Y, Wang X, Wilkinson S (2022) Mechanical, acoustic and thermal performances of Australian Hempcretes. In: Ha-Minh C, Tang AM, Bui TQ, Vu XH, Huynh DVK (eds) CIGOS 2021, Emerging technologies and applications for green infrastructure. Springer Nature Singapore, Singapore, pp 753–761
38. Bies DA, Hansen CH, Howard CQ (2017) Engineering noise control, 5th edn. CRC Press, Boca Raton
39. Cox T, D'Antonio P (2016) Acoustic absorbers and diffusers: theory, design and application. CRC Press, Boca Raton
40. Liu P, Chen G-F (2014) Porous materials: processing and applications. Elsevier, Amsterdam
41. ISO 10534-2 (2023) Acoustics—Determination of acoustic properties in impedance tubes — Part 2:

Two-microphone technique for normal sound absorption coefficient and normal surface impedance, ISO - International Organization for Standardization
42. Tao J, Wang P, Qiu X, Pan J (2015) Static flow resistivity measurements based on the ISO 10534.2 standard impedance tube. Build Environ 94:853–858
43. Niyigena C, Amziane S, Chateauneuf A (2018) Multicriteria analysis demonstrating the impact of shiv on the properties of hemp concrete. Constr Build Mater 160:211–222
44. Chabannes M, Garcia-Diaz E, Clerc L, Benezet JC (2015) Studying the hardening and mechanical performances of rice husk and hemp-based building materials cured under natural and accelerated carbonation. Constr Build Mater 94:105–115
45. Amziane S, Toussaint E, Collet F (2025) RILEM TC 275-HDB: presentation of TC 275-HDB and mechanical performances of the hemp concrete specimens of the interlaboratory comparison. Mater Struct 58:162
46. Bakkour A, Ouldboukhitine S-E, Biwole P, Amziane S (2025) Hygrothermal performance of wood-cement walls across various climate conditions. Mater Struct 58:41
47. Abbas MS, McGregor F, Fabbri A, Ferroukhi MY (2020) The use of pith in the formulation of lightweight bio-based composites: impact on mechanical and hygrothermal properties. Constr Build Mater 259:120573
48. Lagouin M, Magniont C, Sénéchal P, Moonen P, Aubert J-E, Laborel-préneron A (2019) Influence of types of binder and plant aggregates on hygrothermal and mechanical properties of vegetal concretes. Constr Build Mater 222:852–871
49. Moussi YE, Clerc L, Benezet J-C (2022) Design of a novel hybrid rice straw/husk bio-based concrete featuring enhanced mechanical and hygrothermal properties. Waste and Biomass Valoriz 14:345–363
50. Yadav M, Saini A (2022) Opportunities & challenges of hempcrete as a building material for construction: an overview. Mater Today: Proc 65:2021–2028
51. Seng B, Magniont C, Lorente S (2019) Characterization of a precast hemp concrete Part I: Physical and thermal properties. J Build Eng 24:100540
52. Tiwari V, Shukla A, Bose A (2004) Acoustic properties of cenosphere reinforced cement and asphalt concrete. Appl Acoust 65:263–275
53. ASTM C423-23 (2023) Standard Test Method for Sound Absorption and Sound Absorption Coefficients by the Reverberation Room Method, ASTM International, West Conshohocken, PA
54. Delany ME, Bazley EN (1970) Acoustical properties of fibrous absorbent materials. Appl Acoust 3:105–116
55. Cox T (2024) Modelling of acoustic absorbers (https://www.mathworks.com/matlabcentral/fileexchange/54004-modelling-of-acoustic-absorbers), MATLAB Central File Exchange. Retrieved February 2, 2024
56. Kirby R (2014) On the modification of Delany and Bazley fomulae. Appl Acoust 86:47–49
57. Cerezo V (2005) Propriétés mécaniques, thermiques et acoustiques d'un matériau à base de particules végétales: approche expérimentale et modélisation théorique (in French). Institut National des Sciences Appliquées de Lyon (INSA Lyon)
58. Kumar D, Alam M, Zou PXW, Sanjayan JG, Memon RA (2020) Comparative analysis of building insulation material properties and performance. Renew Sustain Energy Rev 131:110038
59. Demirboğa R (2007) Thermal conductivity and compressive strength of concrete incorporation with mineral admixtures. Build Environ 42:2467–2471
60. Dondi M, Mazzanti F, Principi P, Raimondo M, Zanarini G (2004) Thermal conductivity of clay bricks. J Mater Civ Eng 16:8–14
61. Song H, Kim T, Hajimohammadi A, Oh JE, Castel A (2024) Detailed characterisation of hemp and hempcrete pore structures: Effects on thermal and acoustic properties. Cem Concr Res 186:107702
62. Van Riessen A, Rickard W, Sanjayan J (2009) Thermal properties of geopolymers. In: Provis JL, van Deventer JSJ (eds) geopolymers. Woodhead Publishing, pp 315–342
63. Matschei T, Lothenbach B, Glasser FP (2007) The AFm phase in Portland cement. Cem Concr Res 37:118–130
64. Noushini A, Babaee M, Castel A (2016) Suitability of heat-cured low-calcium fly ash-based geopolymer concrete for precast applications. Mag Concr Res 68:163–177
65. Pasupathy K, Berndt M, Sanjayan J, Rajeev P, Cheema DS (2018) Durability performance of precast fly ash-based geopolymer concrete under atmospheric exposure conditions. J Mater Civ Eng 30:04018007
66. Nguyen QD, Afroz S, Zhang Y, Kim T, Li W, Castel A (2022) Autogenous and total shrinkage of limestone calcined clay cement (LC3) concretes. Constr Build Mater 314:125720
67. Zhou Y, Gong G, Xi B, Guo M, Xing F, Chen C (2022) Sustainable lightweight engineered cementitious composites using limestone calcined clay cement (LC3). Compos B Eng 243:110183
68. Sahraei Moghadam A, Omidinasab F, Moazami Goodarzi S (2021) Characterization of concrete containing RCA and GGBFS: mechanical, microstructural and environmental properties. Constr Build Mater 289:123134